npj | 2D Materials and Applications

www.nature.com/npj2dmaterials

ARTICLE OPEN

Degradation of black phosphorus is contingent on UV–blue light exposure

Taimur Ahmed[1], Sivacarendran Balendhran[1], Md Nurul Karim[2], Edwin L. H. Mayes[3], Matthew R. Field[3], Rajesh Ramanathan[2], Mandeep Singh[2], Vipul Bansal[2], Sharath Sriram[1], Madhu Bhaskaran[1] and Sumeet Walia[1]

Layered black phosphorous has recently emerged as a promising candidate for next generation nanoelectronic devices. However, the rapid ambient degradation of mechanically exfoliated black phosphorous poses challenges in its practical implementation in scalable devices. As photo-oxidation has been identified as the main cause of degradation, to-date, the strategies employed to protect black phosphorous have relied upon preventing its exposure to atmospheric oxygen. These strategies inhibit access to the material limiting its use. An understanding of the effect of individual wavelengths of the light spectrum can lead to alternatives that do not require the complete isolation of black phosphorous from ambient environment. Here, we determine the influence of discrete wavelengths ranging from ultraviolet to infrared on the degradation of black phosphorous. It is shown that the ultraviolet component of the spectrum is primarily responsible for the deterioration of black phosphorous in ambient conditions. Based on these results, new insights into the degradation mechanism have been generated which will enable the handling and operating of black phosphorous in standard fabrication laboratory environments.

npj 2D Materials and Applications (2017)1:18 ; doi:10.1038/s41699-017-0023-5

INTRODUCTION

Black-phosphorus (BP) has recently emerged as a material of interest owing to its high carrier mobility and the presence of a direct bandgap.[1] Its thickness-dependent energy gap and highly anisotropic properties make it an important material to investigate from the family of two-dimensional (2D) materials.[2, 3] Exfoliated few-layer BP has been a focus of several studies and is promising for applications in electronics, optoelectronics, energy storage, gas sensing, catalysis and chemical/biosensing.[4–9]

However, any practical implementation of BP is hampered by its susceptibility to ambient conditions.[10, 11] The material degrades rapidly (within few hours to days depending on BP thickness) when exposed to the environment. After a lot of debate, there is a growing consensus that the main cause of BP degradation is photo-oxidation which is expedited in the presence of moisture.[10, 12–15] It is also generally agreed upon that the photodegradation of BP is thickness-dependent. However, there is a mismatch between theoretical and experimental studies in regards to BP stability. A recent study suggests that BP consisting of six or more monolayers is stable for relatively longer periods.[10] This has also been corroborated using theoretical calculations.[13] However, experimental investigations consistently show that even thicker layers of BP are prone to ambient degradation. It is noteworthy that the theoretical models, being resource-intensive, are restricted to mono-layer to few-layer BP, wherein they suggest the involvement of superoxide radicals (O_2^-) as the dominant reactive oxygen species (ROS) participating in BP photo-oxidation.[13] As such, several reports of BP degradation have surfaced recently and passivation procedures are now being explored to protect the material.[16–23]

A knowledge gap exists in terms of (i) which part of the light spectrum degrades BP the most, and (ii) involvement of additional ROS in BP degradation, particularly in the case of thicker BP flakes. Here, we study the effect of discrete wavelengths ranging from ultraviolet (UV) to infrared and the mechanism behind the degradation of mechanically-exfoliated BP flakes of 20–30 nm thickness. The interactions of different wavelengths, their effect on surface morphology, light-activated degradation, and mechanisms to prevent such degradation are explored.

RESULTS

BP flakes are mechanically-exfoliated on to 100 nm SiO_2 on Si substrates. We choose BP flakes 20–30 nm thick so that the involvement of additional ROS in the case of thicker flakes can be assessed and the relative degradation at different wavelengths can be better separated. This is because thin flakes rapidly form a P_xO_y layer at the top surface that makes it complex to assess and compare degradation with varying wavelengths of light.[10] The layered nature of BP can be observed from the transmission electron micrograph (TEM) of a mechanically exfoliated flake (Fig. 1a). Figure 1b shows the selective area electron diffraction (SAED) pattern of the highlighted area, which further signifies the occurrence of perfectly crystalline, pristine BP, whereas Fig. 1c shows a magnified, high resolution TEM (HRTEM) image of the BP flake shown in Fig. 1a. The lattice fringes correlate well with those reported in literature, indicating the presence of crystalline BP.[24, 25] Figure 1d shows a Raman spectrum acquired from a representative BP flake. All three signature peaks of BP corresponding to the 361 cm^{-1} (A^1_g mode), 438 cm^{-1} (B^2_g mode)

[1]Functional Materials and Microsystems Research Group and Micro Nano Research Facility, RMIT University, Melbourne, VIC 3001, Australia; [2]Ian Potter NanoBioSensing Facility, NanoBiotechnology Research Laboratory, School of Science, RMIT University, Melbourne, VIC 3001, Australia and [3]RMIT Microscopy and Microanalysis Facility, RMIT University, Melbourne, VIC 3001, Australia
Correspondence: Sumeet. Walia (sumeet.walia@rmit.edu.au)

Received: 18 January 2017 Revised: 9 June 2017 Accepted: 13 June 2017
Published online: 29 June 2017

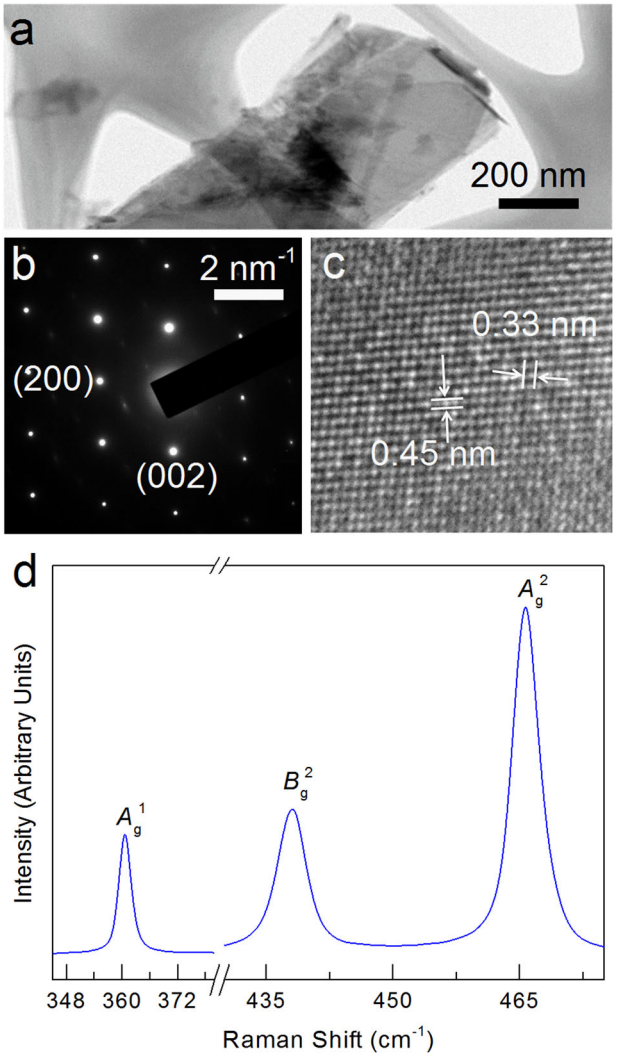

Fig. 1 Characterisation of mechanically-exfoliated black phosphorus. **a** Transmission electron micrograph of a multilayer BP flake. **b** SAED pattern and **c** HRTEM image of the crystal shown in **a**, indicating the presence of crystalline BP. **d** Micro-Raman spectra of a BP flake showing the presence of all three signature BP modes

and 465 cm^{-1} (A^2_g mode) are observed.[2] The A^1_g mode originates primarily from the out-of-plane vibrations of phosphorus atoms along the *c*-axis, while the B^2_g and A^2_g modes arise from the in-plane vibrations of phosphorus atoms along the *b*-axis (armchair) and *a*-axis (zigzag), respectively.[26]

To assess the rate of BP degradation under different wavelengths of light, six representative BP flakes are chosen and atomic force microscopy (AFM) scans are performed prior to exposure as reference. Subsequently, these flakes are individually exposed to six different light wavelengths (280, 455, 565, 660, 850 and 1050 nm corresponding to equivalent energies of 4.43, 2.72, 2.19, 1.88, 1.46 and 1.18 eV, respectively) and imaged after identical exposure durations (30, 60, 90 and 120 min). The intensity of all light sources is maintained at 4.5 mW/cm^2. The exposures are conducted in a dark room to rule out any influence of ambient light. Thereafter, AFM imaging of the BP flakes is conducted immediately after exposure at every time step. Figure 2 shows the evolution of BP degradation for the different photo-wavelength exposures, at varying time durations. After 2 h of exposure, it is seen that predominantly UV (280 nm) followed by blue light (455 nm) are responsible for the appearance of morphological protrusions on the BP surface, which are indicative of material deterioration.[22, 27] None of the BP flakes exposed to green (565 nm), red (660 nm) and infrared (850 and 1050 nm) show any signs of degradation within the same time duration. It is also clear that UV light causes fastest deterioration of the BP surface, whereas blue light induced degradation is comparatively slower. Figure 3a shows the absorbance spectrum of a representative BP flake. It can be observed that there are two absorption bands; one in range of 280–300 nm and another between 370–390 nm with a shoulder in the blue region, which is in line with previous reports.[28] This implies that UV light is readily absorbed by BP along with a component of blue, indicating that the high absorption in UV and blue might be the main factors in the photo-oxidation induced degradation of BP. This agrees with theoretical studies which predict that intrinsic defect induced photo-oxidation sites lower the chemisorption barrier of BP.[29] As such, the onset of photo-oxidation occurs most readily in the UV-blue region.

DISCUSSION

Now we assess the mechanism governing the BP degradation process (schematic illustration in Fig. 3b). It is theoretically predicted that the exposure of up to 3–5 layers thick BP to ambient light and molecular oxygen leads to the generation of superoxide radicals (where the reaction proceeds at −4.11 eV with respect to the vacuum level), which is further expedited in the presence of H_2O.[13, 30–34] The generated superoxide radicals are proposed to interact with the BP surface to produce P_xO_y, resulting in the eventual loss of pristine BP.[10, 13] The process of superoxide radical formation cannot be sustained in BP that is beyond 3–5 layers in thickness due to the changes in the band positions in thicker BP flakes.[13] In this scenario, however, when thicker BP flakes are photoirradiated, they can efficiently participate in the generation of OH$^•$ radicals (reaction proceeds at much lower potential of −4.76 eV with respect to the vacuum level).[13, 33, 34] Further, photoexcitation of BP has been demonstrated to efficiently generate singlet oxygen $^1O_2$, an another ROS.[30] The process of production of these different ROS on photoexcitation is very much similar to photosystem II chemistry in plants, where a combination of light and oxygen in the presence of moisture is known to produce oxidising radicals and ROS, which are detrimental to organisms.[35]

We also hypothesise that discrete components of the light spectrum play drastically different roles in ROS generation, consequently affecting BP degradation. Hence, we need to understand the ROS generation capabilities of the individual components of light, to obtain further insights into the degradation of BP.

Therefore, we perform assays under discrete components of the light spectrum to assess the production of these ROS (see experimental section for details). Figure 3c shows a comparison of the $^1O_2$ and OH$^•$ radicals generated at six different excitation wavelengths used in this study. It is distinctively clear that the relative generation of both $^1O_2$ and OH$^•$ radicals is significantly higher under UV irradiation. An interesting observation is that there is a rapid burst generation of OH$^•$ radicals at lower time points. However, this saturates within 15 min of light exposure. In contrast, there is a gradual increase in the generation of $^1O_2$ up to 15 min following which there is a significant increase in the ROS generation. Such a trend is not observed for either visible or infrared light exposure. Of the other wavelengths that are assessed, blue (455 nm) light resulted in the generation of both singlet oxygen and hydroxyl radicals, albeit with lower efficiency when compared to UV. Wavelengths higher than blue generate negligible ROS. We did not observe any discernible production of superoxide radical under photoexcitation conditions. These results clearly show that UV and blue light can result in the generation of the $^1O_2$ and OH$^•$ radicals, which may facilitate degradation of even thick BP flakes. Since high energy wavelengths are more efficient in producing these ROS, UV light aids

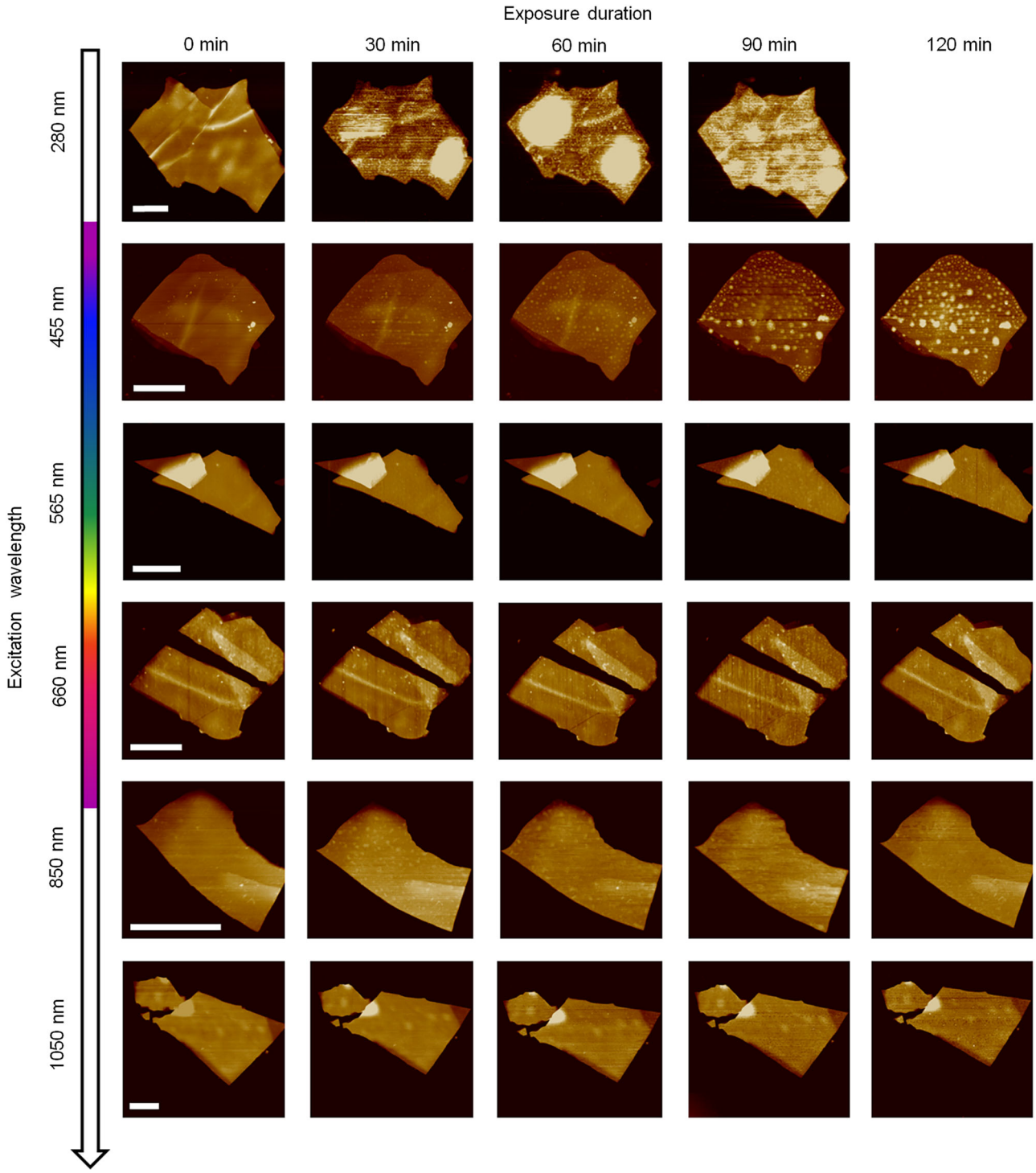

Fig. 2 Atomic force micrographs of BP flakes showing degradation with respect to time, upon exposure to different optical wavelengths. It can be seen that the UV light causes maximum degradation followed by blue light. The degradation is observed by the appearance of bubble-like morphological features on the surface of the flakes. Scalebars denote 1 μm

the rapid degradation of BP in comparison to the rest of the light spectrum. This observation is well in alignment with the AFM analysis (Fig. 2) which suggests UV light to be the predominant contributor towards the photo-induced degradation of BP with some contribution from blue light.

The aforementioned experiments demonstrated that the damaging ROS species are formed within a few minutes of photoexcitation. Hence, we hypothesise that upon exposure to UV, the degradation should occur regardless of subsequent isolation from ambient environment. To verify this, we expose a fresh set of mechanically exfoliated BP flakes to UV and blue light (characterised using AFM prior to exposure, Fig. 4a) for a short duration of 10 min. Subsequently, the flakes are stored in a controlled N_2 environment in dark and then re-imaged after 24 h. A control sample is also stored in a N_2 environment in dark to ensure its comparison with the light-exposed BP flakes. Figure 4a

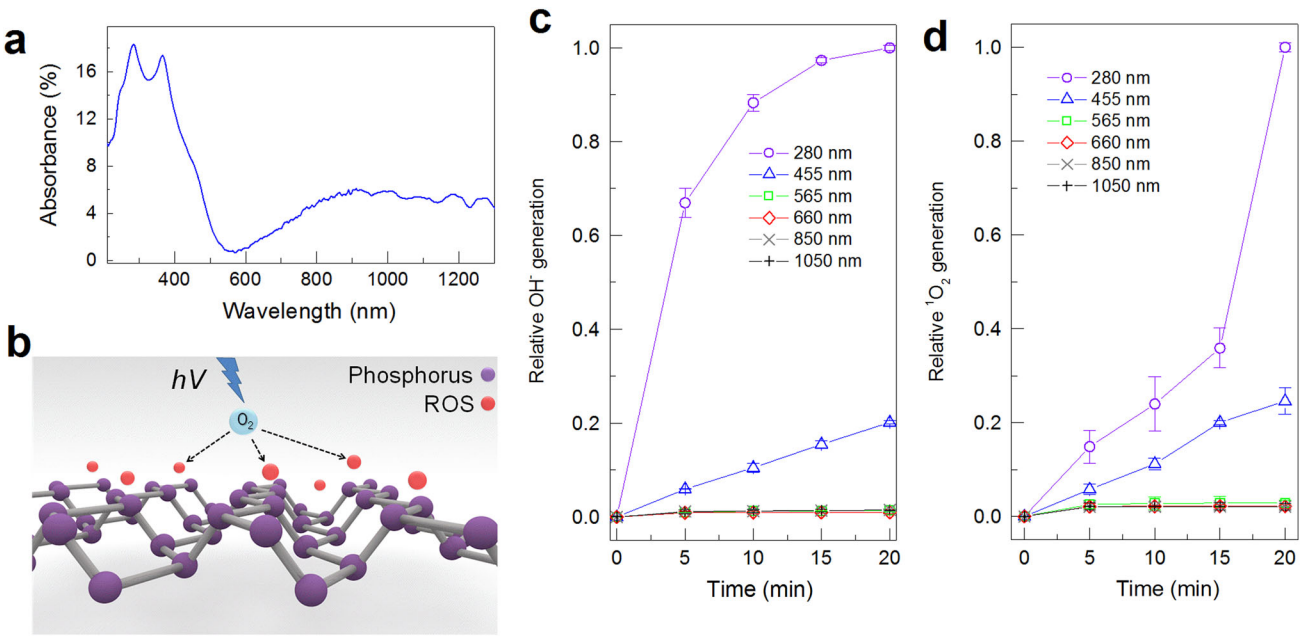

Fig. 3 **a** Absorbance spectrum acquired from a representative mechanically-exfoliated BP flake. It shows two clear bands in the UV region and a shoulder in the blue wavelength. **b** A schematic representation of the photo-oxidation mechanism, whereby reactive oxygen species are generated via the interaction of atmospheric oxygen and light. These reactive oxygen species result in the degradation of BP. **c**, **d** The generation of damaging reactive oxygen species ($^1O_2$ and $OH^•$) under, different excitation wavelengths (see experimental section for details about ROS generation). It is seen that the UV ligh t generates the maximum reactive oxygen species that degrade BP. This is in line with physical observations presented in the AFM results shown in Fig. 2. The error bars in **c**, **d** are standard deviations obtained from three independent experiments with each experiment comprised of four replicates

shows a comparison of AFM scans of the BP flakes which were subjected to short exposure and then stored for 24 h in an inert atmosphere with the control sample. It is seen that the flake that was exposed to UV deteriorated the most, followed by BP exposed to blue (455 nm) light. Higher wavelength exposures did not result in any degradation and appeared similar to the control sample. This observation is in line with expectations that UV and blue light generates ROS within the first few minutes of exposure and subsequently results in degradation of the surface, even if it is subsequently stored under inert conditions.

To confirm that the observed deterioration of BP is not limited only to the surface but also results in a commensurate decline of electronic properties, we measure the current flow through of BP flakes for extended durations, under various excitation wavelengths which can indicate changes in the electronic characteristics as the material deteriorates. The current is acquired at a constant bias of 50 mV on BP flakes with electrodes in a two-terminal configuration (see experimental section for details). The rate of current decay is fastest under 280 nm exposure (Fig. 4b). Minimal or no current decay is observed upon exposure to higher wavelengths even on extended exposures of up to 8 h. The trend in current decay is consistent with our observations; whereby, the BP flakes exposed to UV shows the highest rate of degradation.

To further support our findings, we perform Raman measurements on individual BP flakes after 60 min exposures to red, green, blue and UV light. Figure 4c shows a comparison of the Raman spectra of BP flakes post-exposure to these different wavelengths. The corresponding extended range spectra are shown in Supplementary Fig. S1. The signature BP peaks are seen in all three cases. A relatively small and broad peak can be observed in the 800–900 cm^{-1} range. These additional features are consistent with the Raman vibration modes of different phosphorus oxides and corresponding acidic species.[22, 36–38] Although further investigations are needed to accurately ascertain the exact composition of these oxidised phosphorus species, these signatures affirm that the degradation of the BP surface predominantly occurs due to the UV light. It should be noted that the as-exfoliated BP does not show the presence of these species (Supplementary Fig. S2).

It can be concluded that handling and operating BP in an UV-deficient environment should be sufficient in protecting it against photo-oxidation. To verify this, we prepared and stored two samples: one in ambient conditions and the other in a standard photolithography lab which lacks UV light. The corresponding AFM images can be seen in Fig 4d and e, respectively. It can be seen that the sample prepared and kept in the photolithography lab does not show any signs of degradation even after 28 days, whereas the sample synthesised and stored under ambient conditions show distinct signs of deterioration. This indicates that isolation from UV light is as effective as surface passivation (using capping layers), without requiring complete isolation from molecular oxygen. Moreover, passivation approaches in early stages limits incorporation of BP into devices, with the proposed use in a yellow-light photolithography environment more practical. Final devices can then be passivated for practical use.

In summary, we have studied the individual role of different parts of the light spectrum in the degradation of BP. Using a combination of AFM and electrical characterizations, it is shown that UV is predominantly responsible for the environmental deterioration of BP. Blue light is also observed to cause minor surface deterioration, however the electronic characteristics decay by less than 5% over 8 h of continuous exposure. In contrast, none of the wavelengths beyond blue light result in discernible degradation of the BP surface or its electronic characteristics (less than 1%). These observations are further validated through studying wavelength-dependent photo-induced generation of a number of ROS that can cause degradation of even 20–30 nm thick BP flakes. As such, this work is an important milestone

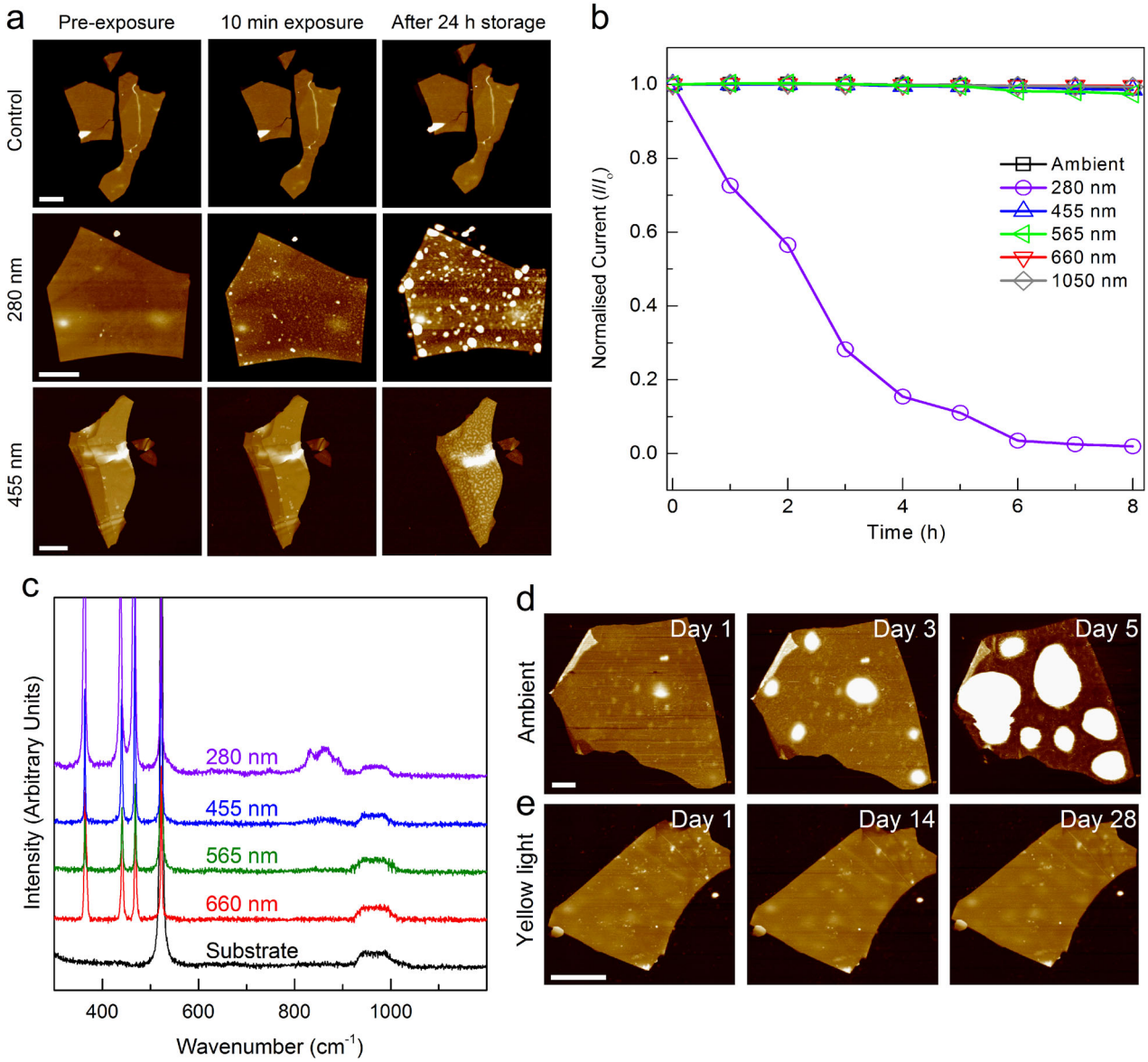

Fig. 4 **a** AFM micrograph on flakes that are initially exposed for only 10 min to 280 nm (UV) and 455 nm (blue), respectively. Subsequently, they are re-imaged after being stored in vacuum for 24 h. The control sample without exposure to UV or blue was left in a N_2 environment in dark for the same duration to compare the degradation with the 10 min light-exposed flakes. The scale bars in **a** represent 1 μm. **b** Current decay with respect to exposure duration for the different wavelengths of light. It is seen that the relative degradation of current is the highest for flakes exposed to 280 nm (UV). **c** Micro-Raman spectra of BP flakes on SiO_2/Si substrates after 60 min exposure to red, green, blue and UV respectively. The evolution of mixed PO_x and H_xPO_y signatures between 800 and 900 cm^{-1} can be observed for blue and UV exposures, whereas these features are absent for higher wavelengths. The corresponding extended range spectra is showm in Figure S1. **d** AFM images of a representative BP flake synthesised and stored under ambient conditions. **e** AFM image of a flake synthesised and stored in a standard photolithography lab that lacks UV light. A comparison of **d**, and **e** shows that the flake in a UV deficient environment remains intact, whereas the flake in ambient shows distinct signs of deterioration in 3 days. The scale bars in **d**, **e** represent 2 μm

towards understanding the underlying mechanisms governing the photo-degradation of BP, whereby it is shown that by isolating BP from UV light it is possible to preserve it without the requirement of inert operating environments.

METHODS

Materials

Layered black phosphorus is obtained via polydimethylsiloxane (PDMS) assisted micromechanical exfoliation of commercial bulk black phosphorus crystals (Smart Elements). Terephthalic acid (TA), 9, 10-anthracenediyl-bis (methylene) dimalonic acid (ABMDMA), rose Bengal (RB), dimethyl sulfoxide, sodium acetate and acetic acid (Sigma-Aldrich, St. Louis, USA) and hydrogen peroxide (H_2O_2, 30% w/w, Chem-Supply Pty. Ltd., Australia) were used in the free radical generation experiments.

Sample fabrication and characterisation

For all the experiments conducted in this work, few-layered black phosphorus crystals were obtained via PDMS assisted micromechanical exfoliation of commercial bulk black phosphorus crystals (Smart Elements).

Instrumentation

Transmission electron microscopy (TEM) images of exfoliated specimens were acquired using a JEOL2100F. AFM imaging is conducted on a Dimension Icon AFM in ScanAsyst mode. The spatial Raman peak intensity

mapping was conducted on a Horiba LabRAM HR Evolution micro-Raman system equipped with 9 mW, 532 nm laser (500 nm lateral resolution, 0.25 s exposure), and a 50 × objective. The representative black phosphorous flakes are exposed to the discrete wavelengths (280, 455, 565, 660, 850 and 1050 nm) by using commercial high power light-emitting diodes (LED, Thorlabs, Inc.). The illumination power was calibrated by a commercial UV-enhanced silicon photodetector (Newport Corporation). Absorption measurements were performed using Envision multilabel plate reader (PerkinElmer). Fluorescence measurements were performed using Fluoromax-4 spectrofluorometer.

Free radical generation

Singlet oxygen radicals were generated by photo-irradiating (intensity of 1.2 mW cm^{-2}) RB dye and the singlet oxygen generation was confirmed through the degradation of ABMBDA dye (0.1 mM ABMDMA with 20 μM RB).[39] ABMDMA, an anthracene derivative, reacts with singlet oxygen to produce an endoperoxide and causes a decrease in the fluorescence intensity at 425 nm[40] which was recorded at 5 min intervals for 20 min by applying an excitation wavelength of 380. The presented data and associated standard deviations are an average of three independent experiments.

The generation of $OH^{\bullet}$ radicals under different light sources was detected using a fluorescent assay. The $OH^{\bullet}$ radical studies were performed in the presence of H_2O_2 (1 M) and TA (1 mM), which was the capture probe.[41] The reaction mixture was independently exposed to the six wavelengths of light (intensity of 4.5 mW cm^{-2}). TA is a non-fluorescent compound that specifically reacts with $OH^{\bullet}$ radicals to form a fluorescent product 2-hydroxyterephthalate (excitation 310 nm; emission 430 nm). The fluorescence intensity was recorded at 5 min intervals for 20 min. The fluorescence intensity is directly proportional to the amount of $OH^{\bullet}$ radicals. The presented data and associated standard deviations are an average of three independent experiments.

BP absorption measurements

A CRAIC 20/30 XL UV-Vis micro-spectrophotometer was used to acquire the absorption profile of the BP flake.

Electrical measurements

Devices were fabricated on mechanically-exfoliated BP flakes on 100 nm SiO_2 on Si substrates. Subsequently, a photoresist layer was spin-coated at 4000 rpm for 45 s followed by 100 °C soft bake. The electrode patterns were UV-exposed using a mask aligner system (MA6, SUSS MicroTech) and subsequently developed. The metal electrodes Cr/Au (10/100 nm) were then deposited on the developed patterns using electron beam evaporation. Finally, the lift-off in acetone was carried out to reveal the required metallic contact pads for micro-probes and electrical measurement. The electrical measurements were conducted using a Keithley 4200SCS semiconductor parameter analyser. All measurements were performed under dark conditions with exposure to only the target wavelength of light.

Data availability

All relevant data is available from the authors on request.

ACKNOWLEDGEMENTS

The authors acknowledge support from the Australian Research Council (ARC) for personnel and project support via DE150100909 (S.B.), DE160100023 (M.B.), DP140100170 (M.B.), DP130100062 (S.S.), FT140101285 (V.B.), DP170103477 (V.B. and R.R.) and equipment funding through LE0882246, LE0989615, LE110100223 and LE150100001. The authors also acknowledge the facilities and technical assistance of the Micro Nano Research Facility (MNRF) and the RMIT Microscopy and Microanalysis Research Facility (RMMF).

AUTHOR CONTRIBUTIONS

T.A. and S.W. conceptualised the study with inputs from S.B., M.B., S.S. and V.B. T.A. and S.B. contributed equally. S.B. and S.W. performed and analysed the Raman data. T.A. and S.W. performed the AFM and electrical measurements. M.N.K, R.R., M.S. and V. B. conducted and analysed the ROS assays. E.L.H.M and M.R.F assisted with TEM measurements. S.W. and T.A. wrote the manuscript with comments and edits from all co-authors.

ADDITIONAL INFORMATION

Supplementary Information accompanies the paper on the *npj 2D Materials and Applications* website (doi:10.1038/s41699-017-0023-5).

Competing interests: The authors declare that they have no competing financial interests.

REFERENCES

1. Ling, X., Wang, H., Huang, S., Xia, F. & Dresselhaus, M. S. The renaissance of black phosphorus. *Proc. Natl Acad. Sci. USA* **112**, 4523–4530 (2015).
2. Zhang, S. et al. Extraordinary photoluminescence and strong temperature/angle-dependent raman responses in few-layer phosphorene. *ACS Nano* **8**, 9590–9596 (2014).
3. Balendhran, S., Walia, S., Nili, H., Sriram, S. & Bhaskaran, M. Elemental analogues of graphene: silicene, germanene, stanene, and phosphorene. *Small* **11**, 640–652 (2015).
4. Chen, Y. et al. Field-effect transistor biosensors with two-dimensional black phosphorus nanosheets. *Biosens. Bioelectron.* **89**, 505–510 (2016).
5. Dai, J. & Xiao, Z. C. Phosphorene, bilayer: effect of stacking order on bandgap and its potential applications in thin-film solar cells. *J. Phys. Chem. Lett.* **5**, 1289–1293 (2014).
6. Li, W., Yang, Y., Zhang, G. & Zhang, Y.-W. Ultrafast and directional diffusion of lithium in phosphorene for high-performance lithium-ion battery. *Nano Lett.* **15**, 1691–1697 (2015).
7. Rahman, M. Z., Kwong, C. W., Davey, K. & Qiao, S. Z. 2D phosphorene as a water splitting photocatalyst: fundamentals to applications. *Energ. Environ. Sci.* **9**, 709–728 (2016).
8. Abbas, A. N. et al. Black phosphorus gas sensors. *ACS Nano* **9**, 5618–5624 (2015).
9. Akhtar, M. et al. Recent Advances in synthesis, properties, and applications of phosphorene. *npj 2D Mater. Appl.* **1**, 5 (2017).
10. Favron, A. et al. Photooxidation and quantum confinement effects in exfoliated black phosphorus. *Nat. Mater.* **14**, 826–832 (2015).
11. Island, J. O., Steele, G. A., van der Zant, H. S. & Castellanos-Gomez, A. Environmental instability of few-layer black phosphorus. *2D Mater.* **2**, 011002 (2015).
12. Walia, S. et al. Defining the role of humidity in the ambient degradation of few-layer black phosphorus. *2D Mater.* **4**, 015025 (2017).
13. Zhou, Q., Chen, Q., Tong, Y. & Wang, J. Light-Induced ambient degradation of few-layer black phosphorus: mechanism and protection. *Angew. Chem.* **128**, 11609–11613 (2016).
14. Hanlon, D. et al. Liquid exfoliation of solvent-stabilized few-layer black phosphorus for applications beyond electronics. *Nat. Commun.* **6**, 8563 (2015).
15. Yau, S.-L., Moffat, T. P., Bard, A. J., Zhang, Z. & Lerner, M. M. STM of the (010) surface of orthorhombic phosphorus. *Chem. Phys. Lett.* **198**, 383–388 (1992).
16. Avsar, A. et al. Air-stable transport in graphene-contacted, fully encapsulated ultrathin black phosphorus-based field-effect transistors. *ACS Nano* **9**, 4138–4145 (2015).
17. Doganov, R. A. et al. Transport properties of pristine few-layer black phosphorus by van der waals passivation in an inert atmosphere. *Nat. Commun.* **6**, 6647 (2015).
18. Edmonds, M. et al. Creating a stable oxide at the surface of black phosphorus. *ACS Appl. Mater. Interfaces* **7**, 14557–14562 (2015).
19. Kang, J. et al. Solvent exfoliation of electronic-grade, two-dimensional black phosphorus. *ACS Nano* **9**, 3596–3604 (2015).
20. Liu, H., Neal, A. T., Si, M., Du, Y. & Peide, D. Y. The effect of dielectric capping on few-layer phosphorene transistors: tuning the schottky barrier heights. *IEEE Electr. Device Lett.* **35**, 795–797 (2014).
21. Pei, J. et al. Producing air-stable monolayers of phosphorene and their defect engineering. *Nat. Commun.* **7**, 10450 (2016).
22. Wood, J. D. et al. Effective passivation of exfoliated black phosphorus transistors against ambient degradation. *Nano Lett.* **14**, 6964–6970 (2014).
23. Walia, S. et al. Ambient protection of few-layer black phosphorus via sequestration of reactive oxygen species. *Adv. Mater.* doi:10.1002/adma.201700152 (2017).
24. Du, Y., Ouyang, C., Shi, S. & Lei, M. Ab initio studies on atomic and electronic structures of black phosphorus. *J. Appl. Phys.* **107**, 093718 (2010).

25. Appalakondaiah, S., Vaitheeswaran, G., Lebegue, S., Christensen, N. E. & Svane, A. Effect of van der waals interactions on the structural and elastic properties of black phosphorus. *Phys. Rev. B* **86**, 035105 (2012).
26. Łapińska, A., Taube, A., Judek, J. & Zdrojek, M. Temperature evolution of phonon properties in few-layer black phosphorus. *J. Phys. Chem. C* **120**, 5265–5270 (2016).
27. Ryder, C. R. et al. Covalent functionalization and passivation of exfoliated black phosphorus via aryl diazonium chemistry. *Nat. Chem.* **8**, 597–602 (2016).
28. Guo, Z. et al. From black phosphorus to phosphorene: basic solvent exfoliation, evolution of raman scattering, and applications to ultrafast photonics. *Adv. Funct. Mater.* **25**, 6996–7002 (2015).
29. Utt, K. L. et al. Intrinsic defects, fluctuations of the local shape, and the photo-oxidation of black phosphorus. *ACS Cent. Sci.* **1**, 320–327 (2015).
30. Wang, H. et al. Ultrathin black phosphorus nanosheets for efficient singlet oxygen generation. *J. Am. Chem. Soc.* **137**, 11376–11382 (2015).
31. Wang, G., Slough, W. J., Pandey, R. & Karna, S. P. Degradation of phosphorene in air: understanding at atomic level. *2D Mater.* **3**, 025011 (2016).
32. Luo, W. et al. Surface chemistry of black phosphorus under a controlled oxidative environment. *Nanotechnology* **27**, 434002 (2016).
33. Krumova K., Cosa G. Overview of reactive oxygen species. In *Singlet oxygen: Applications in Biosciences and Nanosciences*, Vol. 1 (eds Nonell, S. & Flors, C.) 1–21 (Royal Society of Chemistry, 2016).
34. Augusto O., Miyamoto S. Oxygen radicals and related species. In *Principles of Free Radical Biomedicine*, Vol. 1, (eds Pantopoulos, K. & Schipper, H. M.) 19–42. (Nova Science Publishers, 2011).
35. Barber, J. & Andersson, B. Too much of a good thing: light can be bad for photosynthesis. *Trends. Biochem. Sci.* **17**, 61–66 (1992).
36. Kim, J.-S. et al. Toward air-stable multilayer phosphorene thin-films and transistors. *Sci. Rep.* **5**, 8989 (2015).
37. Carbonnière, P. & Pouchan, C. Vibrational spectra for P_4O_6 and P_4O_{10} systems: theoretical study from dft quartic potential and mixed perturbation-variation method. *Chem. Phys. Lett.* **462**, 169–172 (2008).
38. Hanwick, T. J. & Hoffmann, P. Raman spectra of several compounds containing phosphorus. *J. Chem. Phys.* **19**, 708–711 (1951).
39. DeRosa, M. C. & Crutchley, R. J. Photosensitized singlet oxygen and its applications. *Coord. Chem. Rev.* **233**, 351–371 (2002).
40. Kuznetsova, N. et al. New reagents for determination of the quantum efficiency of singlet oxygen generation in aqueous media. *Russ. J. Gen. Chem* **71**, 36–41 (2001).
41. Gomes, A., Fernandes, E. & Lima, J. L. Fluorescence probes used for detection of reactive oxygen species. *J. Biochem. Bioph. Met.* **65**, 45–80 (2005).